EMPLOYING ZINC OXIDE NANOPARTICLE COATING AS A CORROSION INHIBITOR FOR MAGNESIUM ALLOYS IN DISTINCT AQUEOUS ELECTROLYTE

Haewon Byeon[1], V.S. Sreenivasan[2], Amaravadi Rama Krishna[3], Charudatta P. Thosar[4], Shrikant B. Randhavane[4], Deepak Singh Baghel[4,5] and J. Sunil[6*]

[1]College of AI Convergence, Inje University, Gimhae, 50834, Republic of Korea
[2]Department of Mechanical Engineering, Sri Krishna College of Technology, Coimbatore - 641042, Tamil Nadu, India
[3]Faculty of Science and Technology, JSPM University, Pune, India
[4]Department of Civil Engineering, SVKM's Institute of Technology, Dhule, Maharashtra, India
[5]CSIR-4pi, NAL Belur Campus, Bengaluru, Karnataka, India
[5]Academy of Scientific and Innovative Research (AcSIR), Ghaziabad, UP-201002, India
[6]Department of Mechanical Engineering, Annai Vailankanni College of Engineering, Kanyakumari, India

ABSTRACT. In this investigation, zinc oxide nanoparticles were synthesised using a straightforward microwave-assisted technique. Results showed that the synthesised nanoparticles were hexagonal wurtzite ZnO-nanoparticles with a crystallite size of 6.76 nm, as determined by physio-chemical methods. It reveals, at varying magnifications, the irregularly aggregated, spherically shaped sponge-like structure. Using Fourier transform infrared spectroscopy, corresponding functional groups on ZnO surfaces have been observed. According to absorption measurements, the direct optical bandgap is around 3.29 eV. The photoluminescence spectra may be used to detect crystal defects in the ZnO lattice by looking for red emission and blue band edge emission. An investigation into the anticorrosion capabilities of zinc oxide nanoparticles was conducted, which revealed that the particles have beneficial characteristics when coated with magnesium (Mg) substrates. These materials are evaluated for corrosive resistance with and without a protective coating. Results show that coating significantly increased the protection rate under different electrolyte conditions. Compared to bare Mg plate, the charge transfer resistance R_{ct} was increased when ZnO nanoparticles were coated.

KEY WORDS: Zinc oxide nanoparticle, Microwave irradiation, Corrosion resistance, magnesium alloy

INTRODUCTION

Recently, advanced nanomaterials have revolutionized various scientific and technological fields, enabling innovative solutions with enhanced properties and functionalities. Zinc oxide nanoparticles have gathered notable consideration among these materials for their unique physicochemical characteristics and versatile applications [1]. ZnO nanoparticles exhibit remarkable semiconducting, catalytic, and electrochemical properties. Consequently, they are excellent potential candidates for various uses, with sensors, solar cells, photocatalysis, and electrochemical devices. ZnO, a wide-bandgap semiconductor with a unique combination of electronic, catalytic and optical characteristics, has intrigued researchers for decades [2]. These properties are significantly altered at the nanoscale, making ZnO nanoparticles an intriguing platform for tailoring material behaviour for specific applications. Various synthesis methods have been devised to harness the potential of zinc oxide nanoparticles. One such approach that has gained prominence for its efficiency and versatility is the microwave-assisted synthesis technique [3]. Controlled and rapid microwave heating has demonstrated its potential to expedite reaction kinetics, influence crystallinity, and yield nanoparticles through controlled size and

_____

morphology [4]. The synthesis of zinc oxide nanoparticles has evolved to encompass various methods, each tailored to control size, morphology, and crystallinity [5]. One such method that has gained prominence for its simplicity and efficiency is the microwave-assisted synthesis technique. This approach capitalizes on microwave irradiation's rapid and controlled heating characteristics to facilitate the formation of ZnO nanoparticles. Leveraging this technique holds the potential to expedite the synthesis process and yield nanoparticles with well-defined properties, contributing to their successful integration into practical applications [6]. In electrochemistry, incorporating zinc oxide nanoparticles into electrode materials has presented opportunities for improving the efficiency and effectiveness of electrochemical devices. Applying a ZnO nanoparticle coating onto conductive substrates results in a synergistic interaction between the distinct characteristics of the nanoparticles and the substrate, enhancing electrochemical performance [7]. Magnesium (Mg) plates are notable among the array of substrates owing to their conductivity, lightweight characteristics, and possible use in numerous electrochemical systems [8]. The analysis of the behaviour of ZnO-coated Mg plates in various electrolyte conditions is an exciting area of study, as it offers the potential to customize electrochemical performance to correspond with specific applications [9].

This work aims to use a microwave-assisted approach to synthesize ZnO nanoparticles and subsequently apply a coating of these nanoparticles onto magnesium plates to conduct electrochemical studies (Electrochemical impedance spectrometry, linear sweep voltammetry). The Mg plates that have been coated will undergo electrochemical tests in acidic (HCl), basic (KOH), and neutral (NaCl) electrolyte environments to assess their compatibility with an electrochemical workstation. The impacts of zinc oxide nanoparticles on the corrosion performance of magnesium alloys were scrutinized. Furthermore, their physico-chemical characteristics were also characterized by using X-ray diffraction (XRD), an ultraviolet-visible spectrophotometer, scanning electron microscopy (SEM) along with energy-dispersive X-ray spectroscopy (EDX), transmission electron microscope (TEM), particle size analysis (PSA), and scanning probe microscopy (SPM). Zinc acetate [$Zn(CH_3CO_2)_2$], Mg plate (substrate), distilled water, ethanol, potassium hydroxide (KOH), sodium chloride (NaCl), sodium hydroxide (NaOH), hydrochloric acid (HCl), pH meter, microwave oven, and electrochemical cell setup were used. All the chemicals were bought from Merck, and reagents were analytical grade and used without additional purification.

EXPERIMENTAL

Synthesis of zinc oxide nanoparticle

A 100 mL of 0.1 M zinc acetate in distilled water was used to form a precursor solution. Further, slowly added a base (NaOH) drop by drop to the precursor solution while stirring. This led to the precipitation of $Zn(OH)_2$. The mixture was transferred to a microwave-safe container and heated it using a microwave oven (180W) for 30 min, allowed for intermittent cooling and stirring. This microwave-assisted heating process promoted the conversion of $Zn(OH)_2$ to zinc oxide nanoparticles. The heating and cooling process was repeated until the solution turned transparent, indicating the formation of nanoparticles. After synthesis the ZnO nanoparticles was repeatedly washed with distilled water and ethanol to eliminate residual reactants or byproducts. Centrifuged the solution and then resuspend the nanoparticles in a solvent. Then, ultrasonicated to disperse the nanoparticles and break apart any agglomerates, resulting in a more stable nanoparticle suspension. Later, the suspension was placed in a hot air oven (80 °C) and calcinated at 400 °C for 3 hours to obtain ZnO nanoparticles [6].

Electrochemical measurements

The electrochemical impedance spectroscopy (EIS) procedure was utilized to assess the anticorrosive properties of the coating. The study focused on the corrosion characteristics of

magnesium metal via a three-electrode cell configuration. A salt bridge was employed as a reference electrode within the overall setting of a sulfate electrolyte. An investigation of electrochemical corrosion was conducted, with experimentation continuing until reaching the level of the concurrent value. Autolab equipment, namely the PGSTAT302N model manufactured by Metrohm Autolab in the Netherlands, was used for this purpose. Different electrolytes, acidic (HCl), basic (KOH), and neutral (NaCl) were employed. The range of applied potential used to investigate corrosion behaviours ranged from -1.8 to -1 V, with a 5 mV scanning rate. The corrosion current (i_{corr}) and corrosion potential (E_{corr}) were measured by extrapolating the data obtained from the anodic and cathodic regions of the potentiodynamic polarization test, also known as the Tafel plot. A 5-mV amplitude alternating current was used to record the impedance data throughout a frequency spectrum of 0.01 to 100 kHz. The tests were conducted three times to ensure the reliability of the findings.

Characterization techniques

The crystallite nature of the developed nanoparticles was assessed via a Bruker D8 Advance X-ray diffractometer, which was scanned within a 2θ range. Fourier transform infrared spectroscopy (FT-IR) was utilized to validate functional groups. PEIR SPECTRUM ASCII PEDS1.60 was used for FT-IR in the wavenumber 4000-400cm^{-1}. The surface morphology was conducted via scanning electron microscopy (SEM) Bruker (Dektak XT), and the elemental authorization was performed via energy dispersive X-ray examination (EDX) (JEOL-6390, Japan). A Shimadzu 1800 UV–visible DRS spectrophotometer was utilized to get a recording of the ultraviolet (UV) spectrum of the ZnO samples. The electrochemical impedance spectroscopy was done to assess the anticorrosion performance of the zinc oxide sample. The electrochemical experiments were conducted on a PGSTAT302N by Metrohm Autolab (Netherlands) at open circuit potential (OCP) in 1M KOH, 1M HCl and 3.5wt% NaCl aqueous solution within the frequency band of 0.01 to 100,000 Hz.

RESULTS AND DISCUSSION

XRD analysis

An X-ray diffraction pattern was analyzed at room temperature to examine synthesised samples' crystallized phases and structural characteristics; the results are presented in Figure 1(a). ZnO's standard hexagonal wurtzite structure (JCPDS no. 36-1451) with the space group P63mc was equivalent to all detected intensity peak patterns [10]. The prominent peaks that are indexed have been observed at the following degrees: 31.7°, 34.4°, 36.4°, 47.4°, 56.7°, 62.9°, 66.4°, 67.8°, 69°, 72.5°, and 76.8° the positions mentioned above agree to the (100) (002) (101) (102) (110) (103) (200) (112) (201) (004) and (202) planes, respectively. Among all distinct orientations of the hkl planes, the (101) plane orientation reveals the highest intensity [8]. The prominent and distinctive peak in the developed ZnO nanoparticles indicates their high purity and crystallinity. Furthermore, no additional diffraction peaks and phases were seen, indicating that the zinc oxide nanoparticles have a crystalline structure, and it seemed apparent that impurities from other components were absent. The approximation of the crystallite size was accomplished via the Scherrer formula [11].

$$D = \frac{K\lambda}{\beta cos\theta}$$

(1)

where, D - average crystallite size, K - constant (0.94), λ - wavelength (CuKα radiation) (1.5406 Å), ϴ - Bragg's diffraction angle, and β - FWHM of the diffraction peak. The crystallite size has been estimated to be 6.76 nm where the measurement of dislocation density determines the

number of defects in the synthesized samples. The estimation uses the crystallite size (D) value in the following relation [12].

$$\delta = \frac{1}{D2} \tag{2}$$

Microwave heating can promote homogeneous nucleation by providing uniform heating throughout the reaction mixture. It leads to a higher number of nuclei, which compete for the available precursor molecules, resulting in smaller crystal sizes. The effective chemical reaction between sodium hydroxide and zinc acetate dihydrate is facilitated by an appropriate amount of sodium hydroxide, which prevents the particles from aggregating. Figure 1(b) illustrates the Rietveld refinement analysis conducted on ZnO nanoparticles. The FullProf analytical program performs Rietveld refinement on X-ray diffraction patterns in qualitative analysis. The ZnO samples undergo refinement using the Pseudo-Voigt function while maintaining a fixed background [13]. The space group assigned to P63mc, which corresponds to the hexagonal wurtzite structure, has a lattice parameter of $\alpha = \beta = \gamma \neq 90°$. This value has been determined by analysing refinement data obtained from ZnO nanoparticles. The refinement parameters used for the characterization of ZnO nanoparticles are space group (P63mc), structure (standard hexagonal wurtzite), crystallite size (6.76 nm), lattice parameter (3.2533 Å) and lattice strain (0.208%). The refining parameters concur highly with prior research outcomes [14].
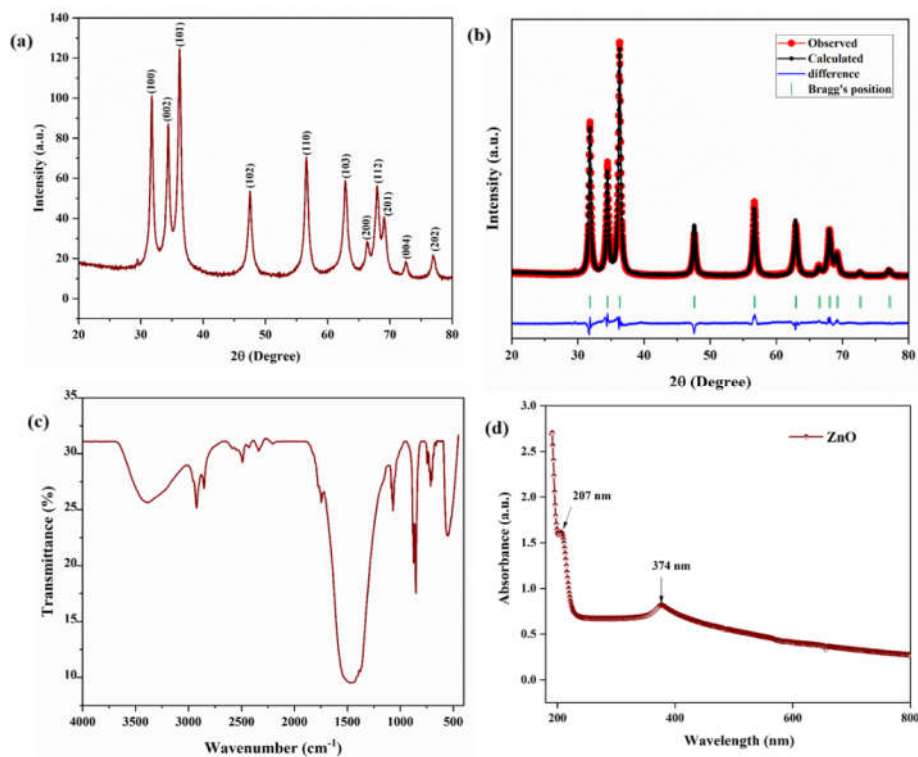

Figure 1. (a) X-ray diffraction pattern of ZnO sample, (b) Rietveld refinement profiles of synthesized ZnO nanoparticle, (c) FT-IR spectra of synthesized ZnO nanoparticle, and (d) UV spectra of prepared ZnO nanoparticle.

Vibrational energy spectra (FT-IR) investigation

The FT-IR spectrum ranges between 4000-400 cm^{-1} in the percent transmittance mode, presented in Figure 1(c). The created ZnO nanoparticles typically show the primary bands and their corresponding regions. The medium peak at 3416 cm^{-1} arises from the hydroxy group [15]. The existence of aromatic aldehydes may be assumed from observing two small absorptions occurring near 2926-2851 cm^{-1}. The broad regions at 1480 cm^{-1} refer to the carbonyl functional groups C=O and C-O, specifically with asymmetric and symmetric stretching vibrations [16]. The wavenumber 1742 cm^{-1} is accredited to the C=O stretching of the aldehyde compound. The wavenumber at 1068 cm^{-1} contributes to stronger C-O stretching of primary alcohol. The absorption band ranging from 854-553 cm^{-1} in the fingerprint area (below 1000 cm^{-1}) is attributed to the stretching mode of ZnO skeletal vibrations [7]. This band exhibits a fundamental frequency with a significant intensity. The study results provide evidence for developing nanostructured zinc oxide (ZnO) particles during their growth phase [4].

Morphology analysis

The SEM study was conducted to investigate the morphology of the synthesized ZnO at various magnifications, as shown in Figure 2(a). In contrast, ZnO nanoparticles prepared revealed the formation of irregularly agglomerated with spherically sponge morphology. When using zinc acetate as a precursor, it is seen that the growth of zinc oxide molecules occurs gradually, resulting in the formation of tiny spherical structures that aggregate in a sponge form.
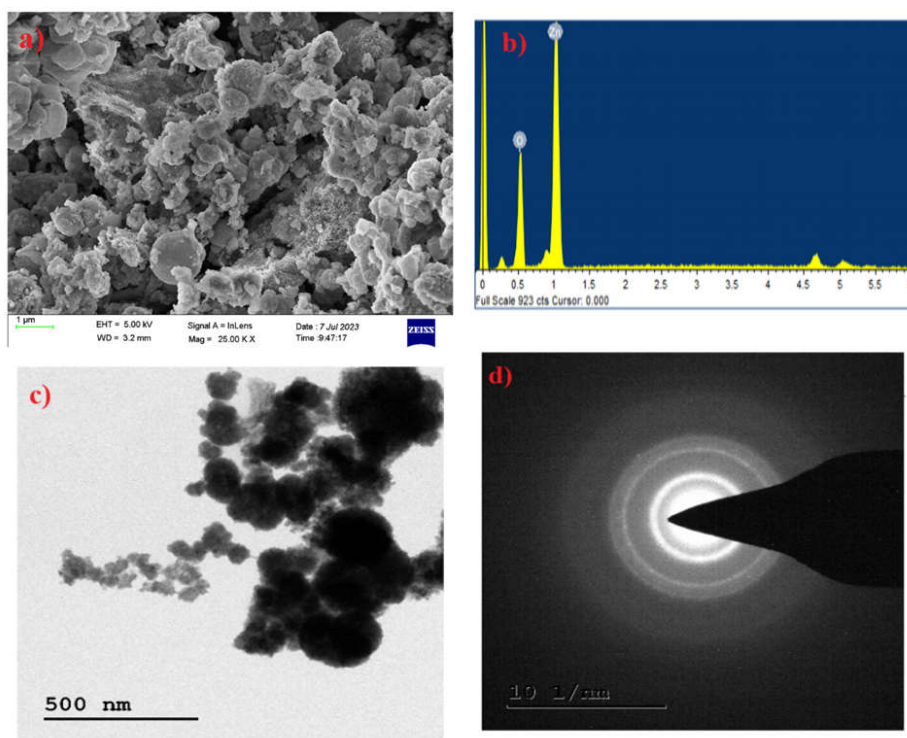

Figure 2. ZnO nanoparticle. (a) SEM image, (b) EDAX, (c) TEM image, and (d) SAED pattern.

The ZnO nanoparticles exhibited a spherical form, which may also be attributed to the thermally activated crystallite development attributable to the fusing of the tiny particles due to the high temperature [17]. The elemental composition was also performed using EDAX analysis, which is revealed in Figure 2(b). Also, it confirms the occurrence of zinc (Zn) and oxygen (O) and reveals the high purity of the prepared zinc oxide nanoparticles. TEM pictures and SAED pattern of microwave-assisted synthesised ZnO samples are shown in Figure 2 (c-d). Spherical-shaped ZnO nanoparticles were obtained at 400 °C. The size of spherical nanoparticles is obtained as 25-50 nm. Compared with other earlier reports, the uniformly distributed spherical-shaped ZnO nanoparticles are obtained in these specified operation procedures. The XRD plots show that the (100) plane has a higher intensity for spherical nanoparticles. Interplanar spacing matches the literature. The SAED pattern shows that the synthesized ZnO nanoparticles are polycrystalline and highly pure [18].

Optical absorption spectra

Figure 1(d) presents the electronic absorption spectrum of ZnO nanoparticles at ambient temperature. This spectrum reveals the absorption edge corresponding to the band structure of the semiconductor. The absorption peaks associated with the zinc acetate precursor are seen at 207 and 374 nm wavelengths, respectively [19]. A prominent peak with an apparent wavelength of around 374 nm indicates ZnO nanoparticles since this characteristic is attributed to their high excitation binding energy under atmosphere circumstances. The presence of ZnO nanoparticles results in an excitonic absorption peak at around 207 nm, a wavelength much lower than the bandgap wavelength of 374 nm ($E_g = 3.29$ eV). The significant acute absorption of ZnO shows the monodispersed characteristics of the particle dispersion [6]. The decreased optical band gap of developed ZnO nanoparticles may be attributable to structural defects during synthesis. The existence of point defects in zinc oxide leads to energy levels inside the bandgap.
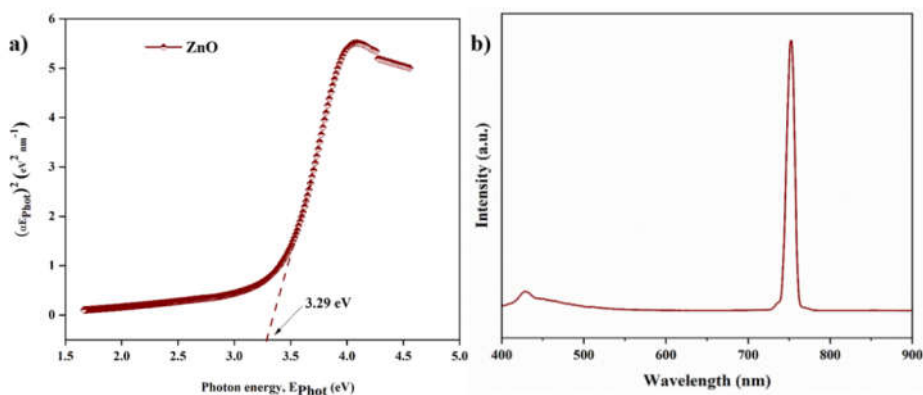

Figure 3. (a) Tauc plot (bandgap) and (b) photoluminescence spectra of synthesized ZnO nanoparticle.

This process contributes to a wide-ranging, profound emission band in the visible spectrum. Using visible light to drive electrons from the valence band to the conduction band in zinc oxide is complex due to the material's high band gap. Four oxygen vacancies in ZnO are necessary for surface imperfections that affect optical absorption in the visible light spectrum [7]. Initially, using primary density functional theory (DFT) simulations, the valence states near the Fermi level

mostly emerge from the O 2p and Zn 3d levels positioned inside the valence band. These particular states induce electronic transitions inside the visible range [17]. The generated ZnO nanoparticles' direct electronic bandgap energy was calculated by extrapolating the linear portion of the graph showing the relationship between the modified Kubelka-Munk function and the photon energy. The graph was used to establish the relationship between the two variables, which was done. The energy band gap value was obtained by the Tauc relation [9]. The Tauc equation was applied to estimate the direct bandgap energy via absorption spectra analysis, as illustrated in Figure 3(a). The absorption coefficient was correlated to the incident photon energy in semiconductor applications using the following equation:

$$\alpha(v)hv = K\left(hv - E_g\right)^n \tag{8}$$

In the equation, $\alpha(v)$ is the absorption coefficient, K - constant, Eg - bandgap energy, hv - incoming photon energy and n remain ½ for direct and two meant for indirect semiconductors. The bandgap calculated is estimated to be 3.29 eV, respectively.

Photoluminescence spectra

The photoluminescence properties of ZnO nanoparticles have been examined by subjecting them to excitation at 300 nm, followed by recording light emission through the wavelength of 400 nm to 900 nm. The photoluminescence (PL) measurements are presented in Figure 3(b). The spectra exhibit a distinctive blue band edge emission at 429 nm, and it was also noticed that the peaks are broad and less intense. Oxygen deficits, zinc interstices, and defects in structure in ZnO nanoparticles were shown to be responsible for the observed deep-level emission. The second significant emission peak was noticed at a wavelength of 751 nm, corresponding to a pure red emission. Hence, the emission occurs through recombination between a singly ionized charge state of destined defects and photo-generated holes, namely oxygen vacancies and zinc interstices.

Tafel polarization

Corrosion parameters and extrapolated Tafel plots were used to assess the corrosion rate of the composite coating developed on the magnesium (Mg) substrate. As indicated, the polarization resistance (Rp) and corrosion rate are recorded in the results in Table 1. Metals corrode because of the cathodic and anodic reaction phenomena. In this case, metal ions are formed or dissolved during the anodic process. If the metal is magnesium-based, mg ions must be removed from the metal surface and into the corrosive solution. An anodic response describes such a unique behaviour. Mg ion creation occurs during the anodic process, whereas OH⁻ is released during the cathodic reaction. Additionally, magnesium ions interact not only with Cl⁻ and OH but also through different elements in the solution. The potentiodynamic polarization curves, commonly known as Tafel plots, for magnesium and Mg-ZnO samples are provided in Figure 4(b), which was created using a 3 M KOH electrolyte solution. Figure 4(b) illustrates that it is abundantly evident where the corrosion potential (E_{corr}) exhibited by the Mg/ZnO sample is shifted towards a higher positive (1.56 V) (anodic area) value for Mg-ZnO in comparison to magnesium (1.64 V). The corrosion current (i_{corr}) was determined to be 2.2421 and 1.8923 x 10^{-4} A cm^{-2} for the magnesium and Mg-ZnO samples, respectively, and reported in Table 1. The findings mentioned above validate that incorporating a thin layer of ZnO spherical nanoparticles onto the surface of the Mg anode effectively reduces the corrosion rate and enhances the electrochemical corrosion resistance.

Figure 4(c) demonstrates the corrosion curves for magnesium and Mg-ZnO in 1 M HCl solution electrolyte. The same pattern of corrosion was seen as well. The corrosion current (i_{corr}) of Mg/ZnO showed a more significant value (0.539 x 10^{-4} A cm^{-2}) than that of Mg (4.1341 x 10^{-4} A cm^{-2}). Figure 4(c) makes it abundantly evident when the corrosion potential (E_{corr}) of the

Mg-ZnO sample is being moved concerning a more positive (-0.80 V) (anodic region) value when related to the value for magnesium (-0.85 V). Figure 4(a) represents the corrosion curve for plate samples of magnesium and magnesium-zinc oxide immersed in a 3.5wt% NaCl electrolyte. The experimental results indicate that the Mg-ZnO sample exhibited a higher corrosion current than the magnesium alloy sample. This observation shows that applying ZnO coating on the surface of Mg enhances corrosion resistance. It was noticed that the Tafel slope had a low potential for magnesium in comparison to Mg-ZnO; this observation suggests that the corrosion rate for magnesium is high.
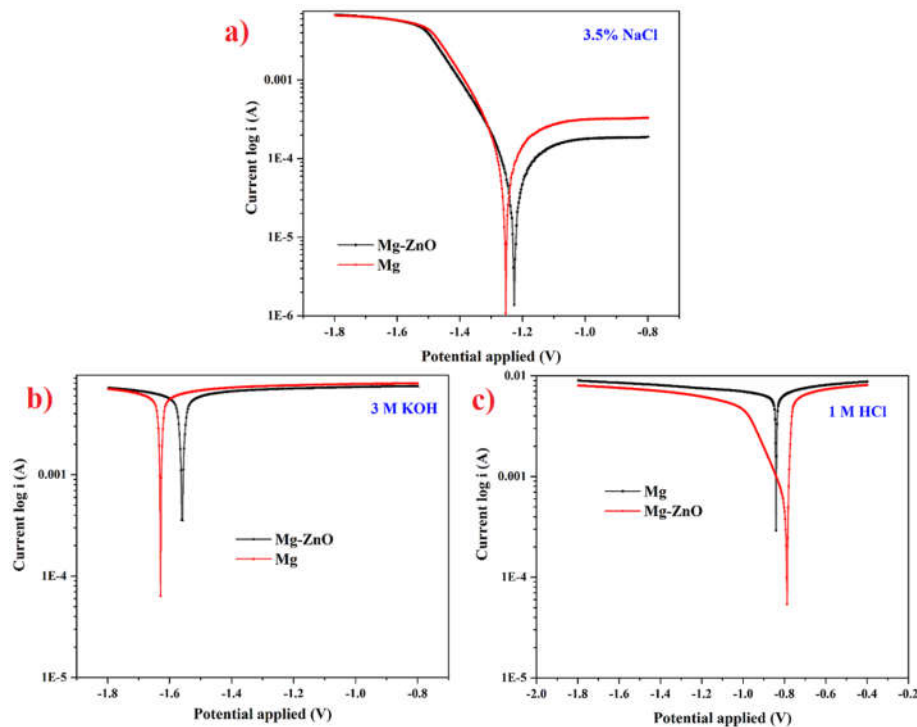

Figure 4. Potentiodynamic polarisation curves of Mg and Mg-ZnO plates under 3.5% NaCl (a), 3 M KOH (b) and 1 M HCl (c) electrolytes.

Table 1. Potentiodynamic polarisation parameters of Mg and Mg-ZnO substrates under three different electrolytes

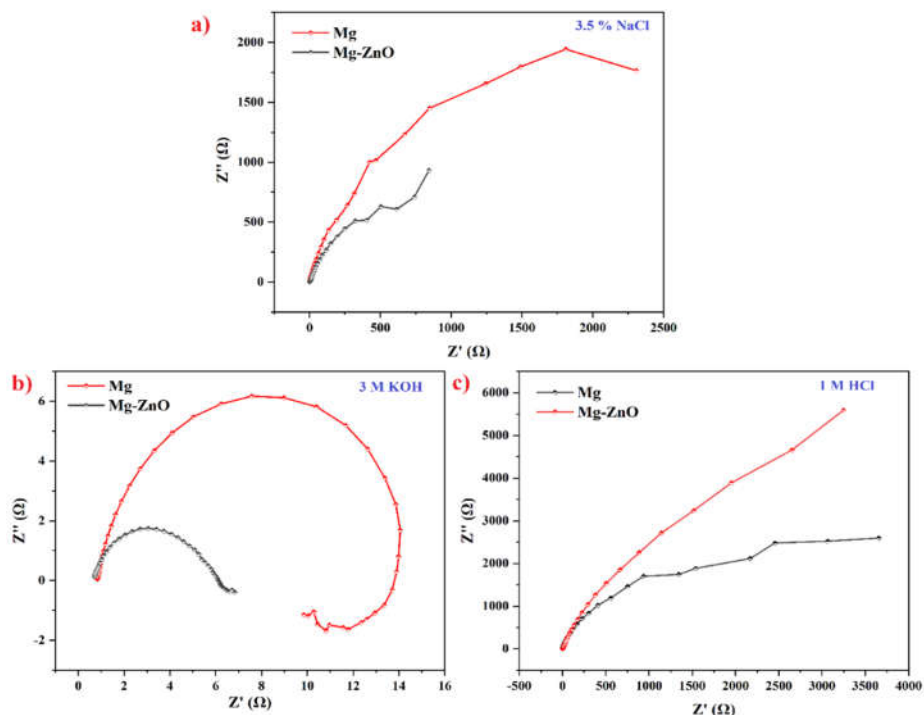| Medium	Substrate	Ecorr (V)	Icorr (A)	Corrosion rate (mm/yr)	Polarization resistance (Ω)	Efficiency (%)
1 M HCl	Mg	-837.65	4.1341	48.038	8.3243	
	Mg-ZnO	-781.86	0.539	6.2743	14.682	86.93
3 M KOH	Mg	-1.5565	2.2421	26.053	7.0847	
	Mg-ZnO	-1.6248	1.8923	12.990	4.9868	50.14
3.5% NaCl	Mg	-1.23	18.068	1.7995	734.14	
	Mg-ZnO	-1.2549	20.044	0.2329	418.15	87.05

Figure 5. Nyquist plot of Mg and Mg-ZnO substrates under three different electrolytes.

The computed corrosion current (i_{corr}) of the magnesium and Mg-ZnO samples has been plotted from the extrapolated lines of the Tafel curve, described in Table 2. The values for these samples were 18.068 and 20.044 x 10^{-4} A cm^{-2}, respectively. Compared to magnesium, which has a corrosion potential of 1.27 volts, the corrosion potential (E_{corr}) of the Mg-ZnO sample, which has a value of 1.23 volts, has shifted toward a value closer to the anodic area. The experiments discussed above demonstrated that a ZnO coating applied to the surface of Mg might significantly increase the material's resistance to corrosion in aqueous solutions [9].

EIS measurements

Corrosion occurs when a corrosive solution penetrates the pores of a material and has a chemical reaction with the substrate. Potentiodynamic polarization was utilized to observe the corrosion resistance effectiveness of the ZnO nanoparticle coating under corrosive circumstances (1 M HCl, 1 M KOH, and 3.5 wt% NaCl solution), as displayed in Figure 5. The resistance of the samples to corrosion was evaluated based on the values of E_{corr} and I_{corr}, which were determined using the Tafel polarization curves and listed in Table 2.

The current density values gradually increase for the coating made on the Mg plate. The E_{corr} values of the ZnO nanoparticle coatings remain up compared to the bare Mg plate, which exhibits a lower value. The I_{corr} value of the bare Mg plate decreases from an order of magnitude lower than that of the ZnO nanoparticle coatings [1]. Electrochemical tests specify the association between the structure of coatings and their microstructures and the corrosion behaviour of the coatings based on observations of the microstructures. Because it constitutes a non-destructive test that does not cause any harm to the sample surface, EIS is one of the electrochemical

Table 2. Electrochemical impedance parameters of Mg and Mg-ZnO substrates under three different
electrolytes.

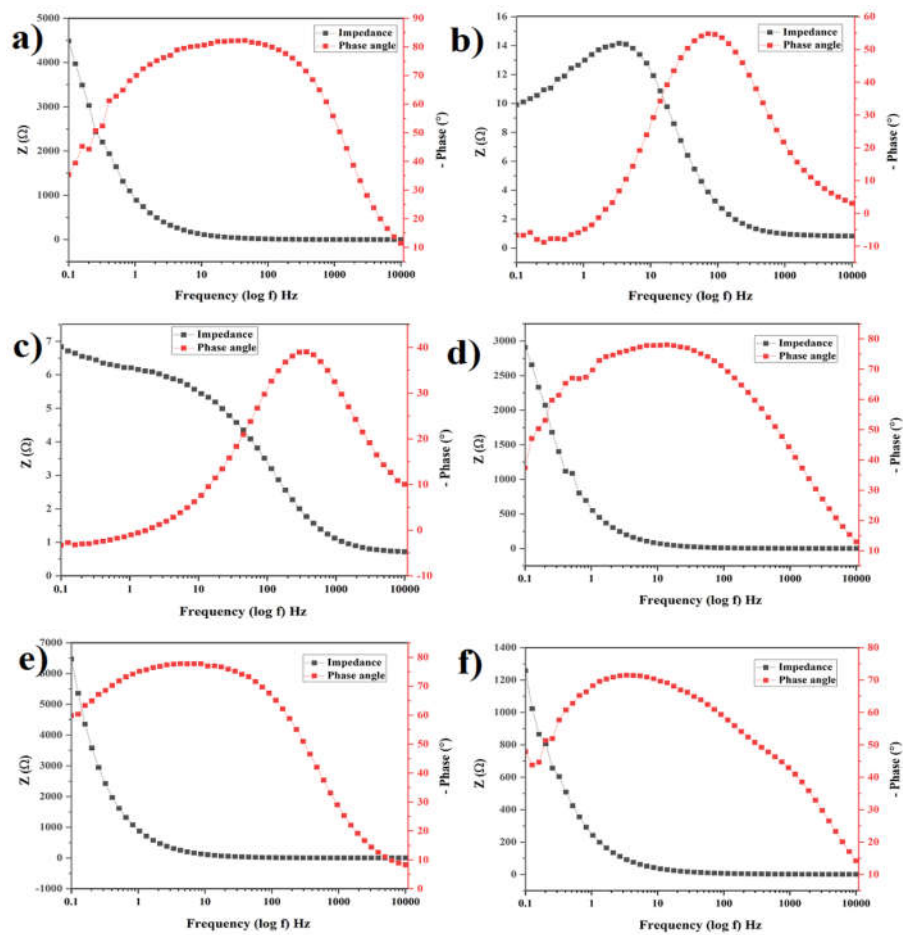| Medium	Substrate	Rs (kΩ)	Rp (mΩ)	CPE.Y0 (μF)	CPE.N (μF)
1 M HCl	Mg	1.2199	5.2971	300.46	0.99716
	Mg-ZnO	3.0348	26.669	55.679	0.99676
3 M KOH	Mg	943.38	4.5454	187.51	0.9983
	Mg-ZnO	823.98	13.613	670.95	0.99892
3.5% NaCl	Mg	758.11	5.3446	297.79	0.99656
	Mg-ZnO	653.54	5.2821	385.94	0.99578

Figure 6. Bode phase and Bode modulus of Mg and Mg-ZnO plates under 3.5 wt.% NaCl (a and b), 3 M KOH (c and d) and 1 M HCl (e and f) electrolyte.

procedures most often used to explore the corrosion process. Figures 5 and 6 show the Bode-phase plots, Bode and Nyquist of coated and uncoated samples, which were acquired using electrochemical impedance spectroscopy (EIS). The coated samples have two loops on their respective Nyquist plots. One has a greater diameter at lower frequencies and is linked to the solution electrolyte interaction with the barrier layer. The other has a smaller diameter at higher frequencies and is connected to the electrolyte contact with the porous oxide layer. Coatings produced on magnesium alloy using zinc oxide nanoparticles have been observed to exhibit similar Nyquist plots [5]. Following Table 2, the corrosion potential of all coated samples was significantly decreased compared to the untreated sample. This indicates that the coated samples had more robust chemical stability when exposed to corrosive solutions. The corrosion potential was initially reduced when nanoparticles were added to the electrolyte, but it subsequently increased following the addition of nanoparticles. Investigating the corrosion current density is the standard method for determining the corrosion rate of the samples; hence, a lower corrosion current density indicates a lower level of corrosion. It is apparent that the ZnO nanoparticle coatings successfully enhance the corrosion resistance of the substrates since all of the coated samples displayed a much lower corrosion current density than the untreated ones.
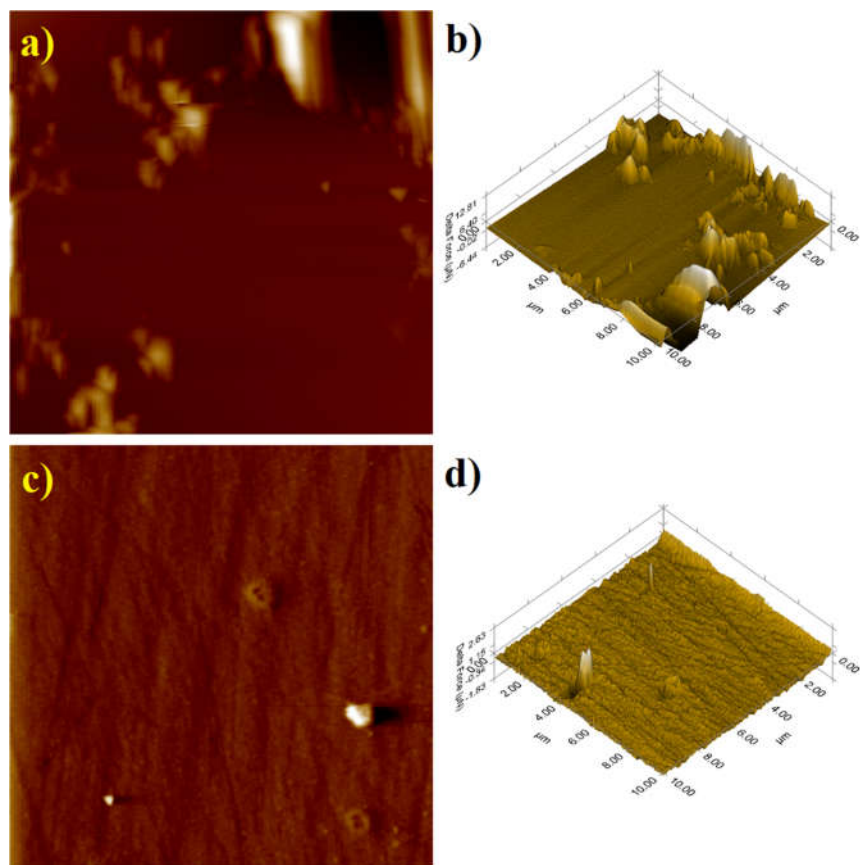

Figure 7. 2D and 3D (topographical images) of Mg and Mg-ZnO plates after LSV and EIS analysis under 3.5wt% NaCl electrolyte.
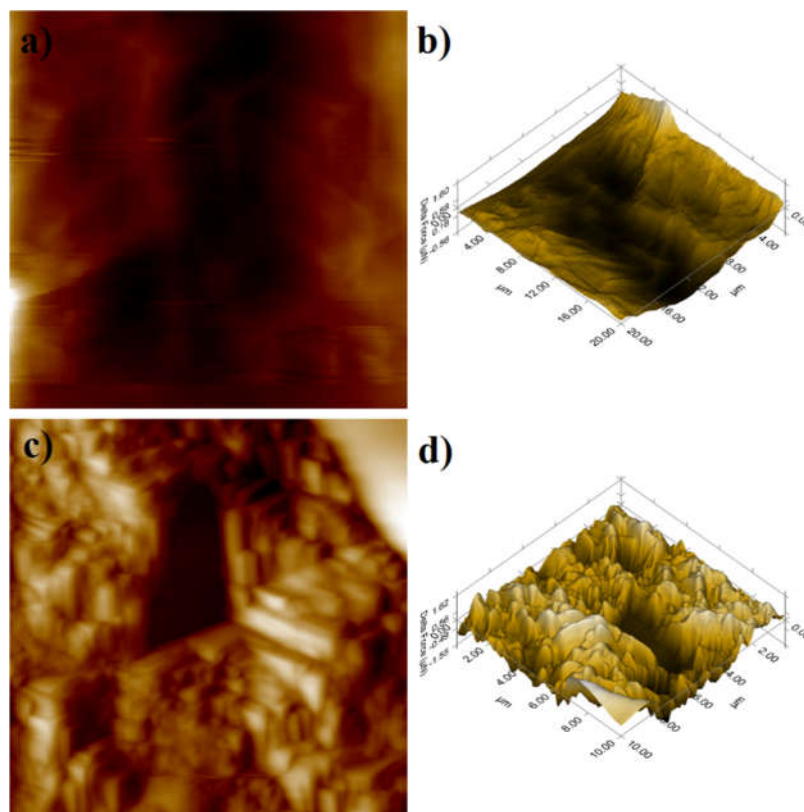
Figure 8. 2D and 3D (topographical images) of Mg and Mg-ZnO plates after LSV and EIS analysis under 1M HCl electrolyte.

Due to the presence of nanoparticles, the impedance of the coated samples increased (in comparison to the uncoated sample), as seen by the Bode plots of both the coated and uncoated samples. The bode phase and bode modulus of the Mg and Mg-ZnO plates under 3.5 wt. % NaCl, 1 M HCl and 3 M KOH electrolyte are shown in Figure 6 (a-f), respectively. Compared to an uncoated sample, which had an impedance of 1.219 cm^2, a coated sample had an impedance of 3.034 cm^2, demonstrating that coatings improved the magnesium alloy's resistance to corrosion. A comparison of a bode plot and a Nyquist plot reveals that the coated samples bode plots have two slopes, which may be understood in terms of the frequency spectrum. Since the Bode-phase plots of coated samples show two peaks, the electrical equivalent circuit (EEC) employed two-time constants to match the EIS data. The magnesium alloy forms an oxide layer at room temperature, exhibiting low corrosion resistance (Rb) and a charge storage capacity (CPEb). The Bode phase and bode modulus of the Mg and Mg-ZnO plates under 3.5wt% NaCl, 3 M KOH and 1 M HCl electrolytes. It shows Bode graphs at varying frequencies, revealing that Mg and Mg-ZnO plates have larger impedance values at lower frequencies. The impedance values are a varying concern to electrolytes and are always higher than uncoated Mg plates for all the electrolytes. These findings from the bode plot and bode modulus show that the corrosion inhibition of the Mg plate is highly enhanced due to the coating of a thin layer of ZnO spherical nanoparticles. Surface topography differences between crystalline and amorphous ZnO sphere

coatings are further shown in Figures 7 and 8 by 3D and 2D photographs acquired utilizing nanoindentation methods. The surface roughness (R_a) after the electrochemical reaction is higher than that before electrochemical reactions. The phenomenon above may also be ascribed to the heightened frequency and quantity of micro-discharges inside conditions characterized by elevated corrosive medium concentrations.

Figure 7 and 8 shows the scanning probe microscope (SPM) topographic images of Mg and Mg-ZnO plates. The hardness and modulus of the Mg-ZnO plates are highly improved than pure Mg plate because of ZnO spherical nanoparticle coatings. The hardness of the Mg-ZnO plate is nearly three times higher than that of the Mg-ZnO plate. After electrochemical analysis, the surface topographical images of Mg and Mg-ZnO plates clearly show the stability of ZnO coatings and valid corrosion protection from aggressive ions, i.e. K, Cl, and OH. The 3D pictures of Mg-ZnO show a nano-globular film structure that vanishes during electrochemical reactions; these micrographs support the FESEM observations of ZnO nanoparticles. Although the specific surface area does not follow any particular trend, the roughness values (R_q and R_a) of Mg increase after corrosion measurement and decrease with coating thickness. It appears that these asperities in the current situation arise during coating but are somehow lessened by the penetration of hostile electrolyte ions. The topographical images revealed the severe damage made by electrolytes during the electrochemical reactions. Even though the surface of Mg plates was successfully protected from the corrosive ions. The surface roughness of the plates is considerably increased compared with uncoated plates. Because uncoated Mg plates can be easily affected by the corrosive ions during the electrochemical analysis, this electrochemical and surface analysis, namely electrochemical impedance spectra, linear sweep voltammetry and nanoindentation techniques, clearly supports the improvement of corrosion resistance of Mg plates by ZnO nanoparticles coating. This finding could be significant and valuable for corrosion prevention research, especially in the Food and automotive industries.

CONCLUSION

The uniformly dispersed spherical zinc oxide nanoparticles were prepared by microwave-assisted chemical method and sodium hydroxide (NaOH) as a reducing agent. The findings obtained through optical microscopy and nanoindentation methodologies were consistent with the stability of ZnO nanoparticle deposition on the surfaces of Mg metal plates. The ZnO nanoparticles synthesized and applied as a coating on Mg metal plates showed remarkable corrosion prevention properties when exposed to a NaCl medium, in contrast to the other electrolyte mediums. The results specify a considerable increase in corrosion resistance of 87.05% when exposed to a 3.5wt% NaCl solution. Similarly, individually, corrosion resistance improves by 50.14%, 86.93%, and 56.8% when subjected to 1 M HCl and 3 M KOH solutions. The surface profiles of the coated plates before and after electrochemical reactions show the excellent stability of the ZnO coating. The results demonstrated that these compounds functioned as very effective corrosion inhibitors for magnesium metal plates when exposed to sodium chloride, hydrochloric acid, and potassium hydroxide solutions.

ACKNOWLEDGEMENTS

REFERENCES

1. Madhumitha, G.; Elango, G.; Roopan, S.M. Biotechnological aspects of ZnO nanoparticles: Overview on synthesis and its applications. *Appl. Microbiol. Biotechnol.* **2016**, 100, 571–581.
2. Hasanpoor, M.; Aliofkhazraei, M.; Delavari, H. Microwave-assisted synthesis of zinc oxide nanoparticles. *Proc. Mat. Sci.* **2015**, 11, 320–325.
3. Sharma, D.; Sharma, S.; Kaith, B.S.; Rajput, J.; Kaur, M. Synthesis of ZnO nanoparticles using surfactant free in-air and microwave method. *Appl. Surf. Sci.* **2011**, 257, 9661–9672.
4. Ong, C.B.; Ng, L.Y.; Mohammad, A.W. A Review of ZnO nanoparticles as solar photocatalysts: synthesis, mechanisms and applications. *Renew. Sust. Energ. Rev.* **2018**, 81, 536–551.
5. Oprea, O.; Andronescu, E.; Ficai, D.; Ficai, A.; N. Oktar, F.; Yetmez, M. ZnO applications and challenges. *Curr. Org. Chem.* **2014**, 18, 192–203.
6. Raha, S.; Ahmaruzzaman, M. ZnO nanostructured materials and their potential applications: Progress, Challenges and perspectives. *Nanoscale Adv.* **2022**, 4, 1868–1925.
7. Bansal, P.; Singh, G.; Sidhu, H.S. Improvement of surface properties and corrosion resistance of Ti13Nb13Zr titanium alloy by plasma-sprayed HA/ZnO coatings for biomedical applications. *Mater. Chem. Phys.* **2021**, 257, 123738.
8. Noman, M.T.; Amor, N.; Petru, M. Synthesis and applications of ZnO nanostructures (ZONSs): A review. *Crit. Rev. Solid State Mater. Sci.* **2022**, 47, 99–141.
9. Kayani, Z.N.; Anjum, M.; Riaz, S.; Naseem, S.; Zeeshan, T. Role of Mn in biological, optical, and magnetic properties ZnO nanoparticles. *Appl. Phys. A: Mater. Sci. Process.* **2020**, 126, 197.
10. Lopes, W.; Ferreira, N.S.; Rodembusch, F.S.; Caldas de Sousa, V. Study of structural and optical properties of ZnO nanoparticles synthesized by an eco-friendly tapioca-assisted route. *Mater. Chem. Phys.* **2021**, 258, 123926.
11. Noei, H.; Qiu, H.; Wang, Y.; Löffler, E.; Woll, C.; Muhler, M. The identification of hydroxyl groups on ZnO nanoparticles by infrared spectroscopy. *Phys. Chem. Chem. Phys.* **2008**, 10, 7092–7097.
12. Xiong, G.; Pal, U.; Serrano, J.G.; Ucer, K.B.; Williams, R.T. Photoluminesence and FTIR study of ZnO nanoparticles: The impurity and defect perspective. *Phys. Status Solidi. C* **2006**, 3, 3577–3581.
13. Janaki, A.C.; Sailatha, E.; Gunasekaran, S. Synthesis, characteristics and antimicrobial activity of ZnO nanoparticles. *Spectrochim. Acta A Mol. Biomol. Spectrosc.* **2015**, 144, 17–22.
14. Talebian, N.; Amininezhad, S.M.; Doudi, M. Controllable synthesis of ZnO nanoparticles and their morphology-dependent antibacterial and optical properties. *Photochem. Photobiol. B* **2013**, 120, 66–73.
15. Yu, J.; Li, C.; Liu, S. Effect of PSS on morphology and optical properties of ZnO. *J. Colloid Interface Sci.* **2008**, 326, 433–438.
16. Zhang, T.; Li, M.; Chen, J.; Wang, Y.; Miao, L.; Lu, Y.; He, Y. Multi-component ZnO alloys: Bandgap engineering, hetero-structures, and optoelectronic devices. *Mater. Sci. Eng. R Rep.* **2022**, 147, 100661.
17. Alias, S.S.; Ismail, A.B.; Mohamad, A.A. Effect of pH on ZnO nanoparticle properties synthesized by sol–gel centrifugation. *J. Alloys Compd.* **2010**, 499, 231–237.
18. Talam, S.; Karumuri, S.R.; Gunnam, N. Synthesis, characterization, and spectroscopic properties of ZnO nanoparticles. *ISRN Nanotechnol.* **2012**, *2012*, 1–6.
19. Long, W.; Yang, Z.; Fan, X.; Yang, B.; Zhao, Z.; Jing, J. The effects of carbon coating on the electrochemical performances of ZnO in Ni–Zn secondary batteries. *Electrochim. Acta* **2013**, *105*, 40–46.